

Design of a ring-shaped traveling-wave Zeeman decelerator for both light and heavy moleculesYabing Ji ¹, Qing Liu,¹ Yang Liu ², Tao Yang,^{1,3,4} Shunyong Hou,^{1,*} and Jianping Yin^{1,†}¹*State Key Laboratory of Precision Spectroscopy, East China Normal University, Shanghai 200241, China*²*School of Physics and Astronomy, Sun Yat-Sen University, Zhuhai 519082, China*³*Collaborative Innovation Center of Extreme Optics, Shanxi University, Taiyuan, Shanxi 030006, China*⁴*Xinjiang Astronomical Observatory, Chinese Academy of Sciences, 150 Science 1 – Street, Urumqi, Xinjiang 830011, China*

(Received 23 May 2023; accepted 3 October 2023; published 30 October 2023)

Taming a broader range of molecular species with large density has been a long-standing goal in molecular science. Heavy molecules with masses greater than 100 amu are of particular interest for precision measurements. However, decelerating a fast-moving beam of such heavy molecules to rest remains challenging for Zeeman deceleration. Moreover, the traditional approach of pulsed Zeeman decelerator suffers from serious molecular loss during deceleration, significantly limiting its potential applications. Herein, we present a proposal of ring-shaped traveling wave Zeeman decelerator (RTWZD) featured with true three-dimensional smoothly moving magnetic potential wells that effectively solve the above intractable problems. With the RTWZD approach, not only can the density of the molecule be greatly increased but also the range of molecular species for Zeeman deceleration can be extended from light to heavy. The performances of the RTWZD are characterized by theoretical analysis and numerical simulations, utilizing a group of atoms and molecules such as ${}^7\text{Li}$, ${}^{16}\text{O}_2$, ${}^{88}\text{Sr}$, ${}^{19}\text{F}$, and ${}^{174}\text{Yb}$ ${}^{19}\text{F}$ as testers. Notably, losses encountered in the traditional Zeeman decelerator can be avoided, yielding more than two orders of magnitude improvement in molecular density. These characteristics of the RTWZD make it an ideal toolbox to produce cold and dense atomic/molecular samples, with promising prospects for cold collision, sympathetic cooling, and precision measurement.

DOI: [10.1103/PhysRevA.108.043115](https://doi.org/10.1103/PhysRevA.108.043115)**I. INTRODUCTION**

Due to their large number of degrees of freedom, long-range interactions, and many unique properties, cold molecules have attracted keen interest in the last two decades [1]. With cold molecules, a wealth of applications can be enabled. Test of fundamental theories in physics and chemistry have been explored with unprecedented precisions [2,3], such as search for the permanent electric dipole moment of electrons (eEDM) [4] and a possible time-dependent variation of fundamental constants of nature [5,6]. Cold molecules are also one of the most promising candidates for quantum computation [7] and quantum simulation [8]. Since the preparation of the first cold gaseous molecular sample [9], there has been an explosion of technical development in producing cold and dense molecules. A variety of methods for cooling and manipulating molecules have been established, including buffer gas cooling [10,11], velocity filtering [12–14], rotational methods (pulsed [15] and quasi-continuous [16]), Stark/Zeman/Rydberg/optical deceleration [17–20], laser cooling [21], evaporative cooling [22], synthetic methods [23,24], and so on. These methods allow for the preparation of molecular samples with temperatures ranging from cold (<1 K) to ultracold (<1 mK), even to quantum

degeneracy domains, and provide access to complete control over all degrees of freedom of the molecule [25].

Most of the cooling techniques mentioned above initiated by molecular beams, some of which exhibit supersonic characteristics. Generally, a supersonic molecular beam is formed via a strong cooling process, resulting in an internally (both vibrationally and rotationally) cooled dense beam [26], which comes at the expense of large forward velocity (typically ranging from 300 m/s to 2000 m/s depending on the carrier gas). In the cold atomic realm, fast-moving beams are usually slowed down by laser cooling. However, laser cooling is not easily applied to molecules because of the lack of a closed two-level scheme for recycling the population in their complicate internal structures, despite population recycling being realized with complicated multiple levels for a select handful molecules in the last decade [21]. Thanks to their electric/magnetic dipole moments, Stark/Zeman deceleration techniques have emerged as important tools for slowing down fast-moving beams of polar/paramagnetic molecules. Zeeman deceleration for paramagnetic molecules has been performed with a traditional pulsed Zeeman decelerator (TPZD), which consists of one-dimensional array of solenoids [18]. Ideally, such a decelerator could keep molecular packets in stable phase space regions without any loss in the deceleration process. Unfortunately, it encounters severe loss of molecules due to the coupling between the transverse and longitudinal motions [27,28]. Molecules initially in the stable region of phase space become unstable and cannot reach the end of the decelerators, especially in the case of long structures [28,29].

*syhou@lps.ecnu.edu.cn

†jpyin@phy.ecnu.edu.cn

Consequently, significant efforts have been devoted to circumventing these intractable problems. For polar molecules, the traveling wave Stark decelerator (TWSD) has been demonstrated on a chip [30] and then expanded to a macroscopic Stark decelerator [31]. It allows for stopping both light [32] and heavy polar molecules [33] and minimizes losses in the deceleration process.

For paramagnetic molecules, there are two approaches adopted to maximize the number of particles that can be decelerated. The first approach involves improving the decelerator structure or altering the operating time sequence for switching the coils. For instance, an alternating arrangement of deceleration and focusing [34], or an evolutionary strategy for generating an optimal time sequence [35] have been used, both of which reduce the coupling between the longitudinal and transverse motions. Nevertheless, this approach cannot fundamentally solve the problem. The second approach involves generating true three-dimensional (3D) magnetic potentials in the decelerator, which can be realized by changing the operation manner and/or the shape of coils. For example, a comoving Zeeman decelerator (CMZD) based on an array of pairwise solenoids generates a series of genuine 3D moving traps for paramagnetic species [36,37]. While a different design of a traveling wave Zeeman decelerator (TWZD) has been demonstrated, where two sets of planar zigzag-patterned wires produce sinusoidal potential along the longitudinal axis and additional quadrupole coils generate transverse magnetic fields (here referred to as zigzag-patterned TWZD) [38,39]. Most recently D. Zhang et al realized a novel TWZD based on a double-helix coil geometry (referred to as double-helix TWZD) [40,41]. Such an approach exhibits full 3D confinement of molecules and gives rise to an improvement of the overall phase space acceptance, leading to larger density of the decelerated molecules. Despite these successes, only a few light paramagnetic species such as H and D atoms [42], metastable He [34,43], metastable $a^3\Sigma_u^+$ He₂ [44], metastable Ne [36,45], metastable Ar [37], metastable N [46], C [47], O and O₂ [37,48–50], NH [51], NO [52], CH₃ [53,54] and OH [41], have been decelerated so far. While some of the Zeeman decelerators, such as CMZD, have the potential to tame heavy molecules, it has not been reported yet, and the density achieved so far is not large enough for the studies of cold reaction.

In this paper, we propose a ring-shaped traveling wave Zeeman decelerator (RTWZD), which effectively addresses the two issues mentioned above. First, it overcomes the issue of particle losses occurred in traditional Zeeman decelerator as a result of its true 3D smoothly-moving potentials, leading to a density more than two orders of magnitude greater than the traditional Zeeman decelerator. Note that, throughout the paper unless otherwise stated, the traditional Zeeman decelerator specifically refers to the unimproved first-generation pulsed Zeeman decelerator. Second, the RTWZD enables decelerating heavy paramagnetic molecules to stand still due to its large and highly stable phase space acceptance. These advantages have important implications for a broad range of applications, including precision measurements [1] and cold collision studies [55,56]. Specifically, in the search of eEDM, the sensitivity scales with the mass of the candidate molecule and the third power of the molecular number [57]. Further-

more, the RTWZD is capable of simultaneously decelerating mixtures of atomic and/or molecular species to any desired velocity and direct trapping of them at the end of the structure, avoiding the loading loss associated with the traditional decelerator. The performance of the proposed RTWZD is studied in detail using both theoretical analysis and numerical simulation, where a group of atoms and molecules are tested, including ⁷Li, ¹⁶O₂, ⁸⁸Sr ¹⁹F, and ¹⁷⁴Yb ¹⁹F. Quantitative comparisons with other types of Zeeman decelerator are also carried out.

II. DESIGN AND FEASIBILITY ANALYSIS

A. Design

The schematic diagram of our proposed ring-shaped traveling wave Zeeman decelerator, depicted in Fig. 1, exhibits a configuration that consists of an assemblage of coils arranged in an array, which are powered by a series of sinusoidally modulated currents. Here, we fully adopted the coil design of the Raizen group [58], namely, the electromagnetic coils have 30 (5 × 6) copper windings (0.5 mm wire diameter), and the current $I_0 = 750$ A. The coils have a length of 3 mm and are positioned at a center-to-center distance of $L = 4.0$ mm, with a gap of 1.0 mm between each coil. The inner and outer diameters of the coil are 10 mm and 15 mm, respectively. All coils in the decelerator are serially connected, with every sixth coil being connected to a current source, for instance, the first coil connects to the seventh coil, the second coil connects to the eighth coil, etc. The current is expressed as $I_n = (-1)^n I_0 / 2 [\cos(2\pi n/N + \phi(t)) + 1]$, with positive and negative currents being applied to even and odd coils, respectively. Here I_0 is the amplitude of the wave form, n represents the n th coil in the decelerator and N is periodicity. The phase offset $\phi(t)$ of the wave form is time-dependent and is given by $\phi(t) = 2\pi \int_0^t \nu(\tau) d\tau$, with the frequency $\nu(\tau)$ being the modulation frequency of the current on each individual coil. The periodicity of our Zeeman decelerator is $N = 6$, which results in a period length of 24 mm. The phase difference of adjacent coils within each polarity set is $2\pi/3$. Under these settings, a periodic array of true 3D potential wells is formed in the Zeeman decelerator and move continuously along the longitudinal axis. Because one oscillation of the wave form moves the potential well over one period, the speed of the potential well is $6L \cdot \nu(\tau)$, which can be changed by chirping the modulation frequency of the currents. We initially set the modulation frequency to match the velocity of the input molecular beam and then gradually reduce it, leading to the deceleration and ultimate stopping of both the wells and the molecules in it.

Figure 2 presents the calculated magnetic field distribution along the cylindrical axis of the coil at five selected moments of $\phi(t) = 0$, $\phi(t) = \pi/6$, $\phi(t) = 2\pi/6$, $\phi(t) = 3\pi/6$ and $\phi(t) = 4\pi/6$, which indicates how the potential wells pass through the subsequent two coils, covering exactly a distance of $2L$. By passing a peak current of 750 A, the decelerator yields a maximum magnetic field as high as 1.4 Tesla along the cylindrical axis, corresponding to a trap depth of approximately 1.7 K for O₂ in the state of $|X^3\Sigma_g^-, N = 1, J = 2, M_J = 2\rangle$.

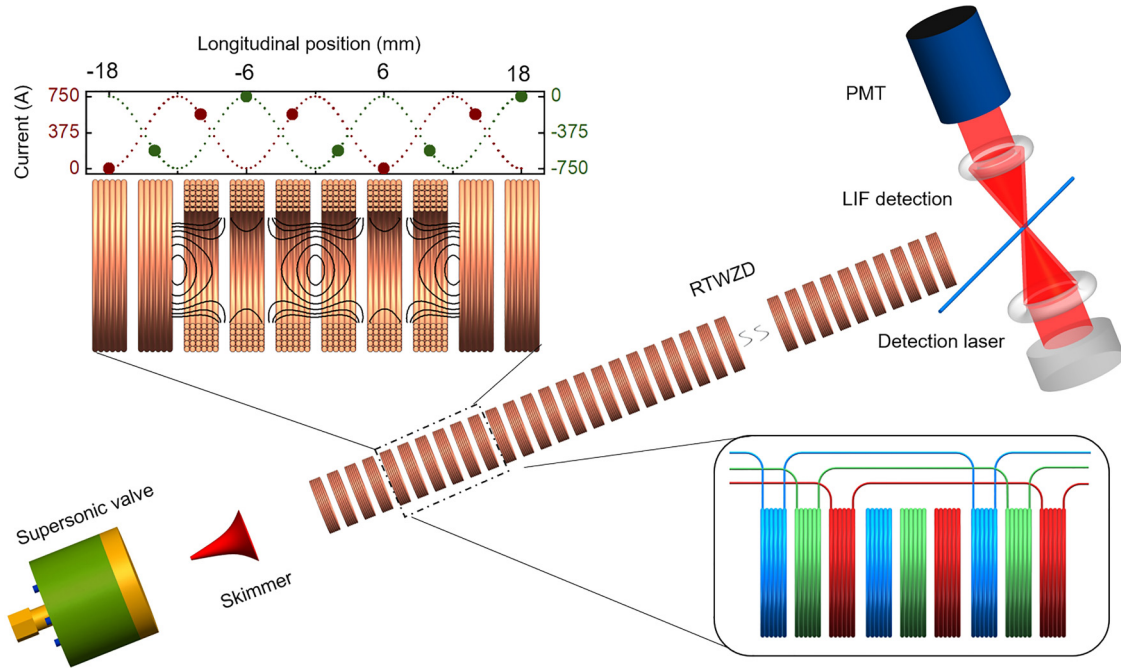


FIG. 1. Proposed setup of the ring-shaped traveling wave Zeeman decelerator. A pulsed supersonic beam produced by a pulsed valve passes through a skimmer and subsequently a part of them is captured by the moving potential wells in the decelerator. In the top inset, a snapshot of the magnetic field contour within the decelerator at a particular moment is provided, where red and green lines present currents with different directions. The bottom inset illustrates the connection of the coils within the decelerator (the leads of the middle three ones are not shown for clarity).

B. Dynamic analysis

The longitudinal motion of molecules relative to the moving potential well is described by

$$m\Delta\ddot{z}_i + ma - \bar{F}(\Delta z) = 0 \quad (1)$$

where m is the molecular mass and Δz is the instantaneous longitudinal position difference between the molecule and the potential well center. Here $a = (v_f^2 - v_i^2)/2S$ is the acceleration of the potential well, with S , v_i , v_f being the distance that the potential well travels, the initial and final velocity of the potential well, respectively. $\bar{F}(\Delta z)$ presents the average force experienced by molecules in the potential well over one period and can be written as a Fourier series

$$\begin{aligned} \bar{F}(\Delta z) = & c_1 \sin(\Delta z\pi/2L) + c_2 \sin(2\Delta z\pi/2L) \\ & + c_3 \sin(3\Delta z\pi/2L) + \dots, \end{aligned} \quad (2)$$

where c_i is the coefficient. By integrating Eq. (1) the potential well in the moving reference frame can be achieved, as shown in Fig. 3. It displays the deceleration dependence of the pseudopotential well experienced by an O_2 molecule in a 1-meter-long RTWZD, corresponding to different final velocities of the moving trap. The longitudinal potential well depth gradually decreases as acceleration increases, indicating that fewer molecules with lower temperatures and lower final velocities will be captured by the decelerator.

As can be seen from Fig. 2, the depth of the transverse potential well varies with the longitudinal position z , resulting in the transverse force felt by a molecule (except on the beam axis) being heavily dependent on its longitudinal position. An average transverse force is introduced to characterize the

transverse motion and is expressed as

$$\bar{F}_t(\phi) = \frac{1}{2L} \int_{\phi L/\pi}^{(\phi+2\pi)L/\pi} F_t(z) dz. \quad (3)$$

The transverse motion of the molecules in the moving frame is given by

$$m\ddot{r}_t - \bar{F}_t(\phi) = 0 \quad (4)$$

The phase space acceptance of the Zeeman decelerator can be achieved by integrating Eqs. (1) and (4), as shown in Fig. 4(d). The potential wells formed in the RTWZD are cylindrically symmetric around the cylindrical axis and the magnetic fields radially increase apart from the axis, molecules in the low-field-seeking states are transversely focused in the deceleration process. Combined with the longitudinal confinement, a conclusion can be drawn that the RTWZD is capable of generating true 3D potential wells in operation.

C. Feasibility analysis

The current chirping technology has been extensively utilized in TWZDs [38–40], which, in principle, can be expanded to the RTWZD. It should be noted that the power electronics of the RTWZD needs to be carefully designed. If all the coils are connected in series, it will be a challenge to the power supply of the device. The strategy of modular design is commonly used in existing TWZDs, where each module produces only several periods of sinusoidal wave form and is opened successively in time. Based on the modular design, we propose an alternative operation strategy, by which only

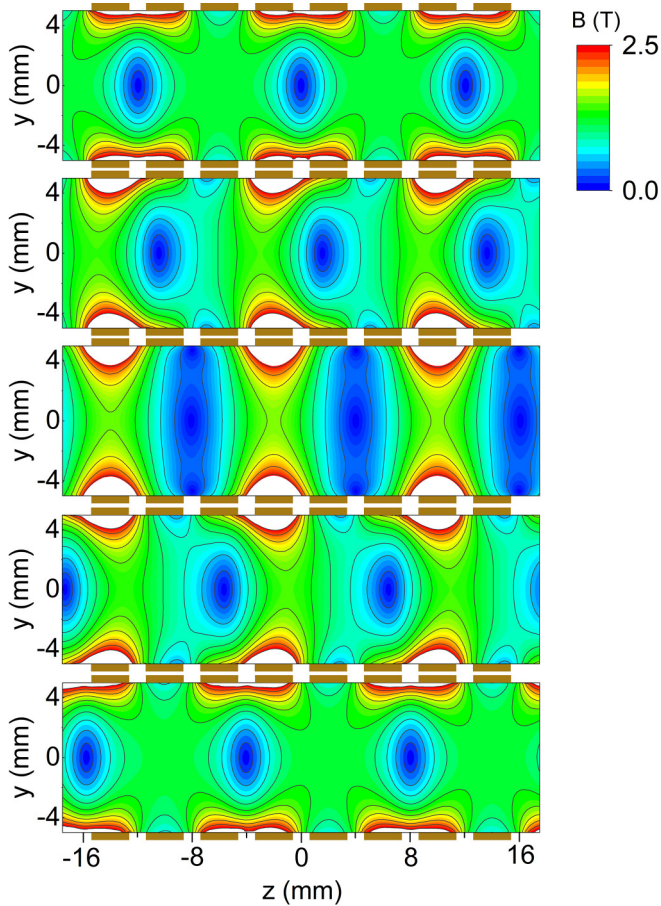


FIG. 2. Distribution of magnetic field strength in the plane containing the cylindrical axis of the coil at five selected moments of the moving potential wells. The potential wells travel a distance of two coils, i.e., $2L$, from top to bottom panel. The copper labels around each magnetic field represent coils.

12 coils are activated in our Zeeman decelerator at any given time. In this method, each module only contains four coils, two thirds of one period, which can greatly reduce the power requirement of the decelerator. All modules, separated by relays, are connected in parallel to the power and only three adjacent modules of them are energized at the same time. When the synchronous molecule passes by the end of the second module of the three energized ones, the first energized one is switched off and the next (not yet activated) module is switched on simultaneously. In this way, there are at least four coils on the front and back ends of the synchronous molecule at any given time, which ensures an ideal distribution of the magnetic field. This also implies each coil needs keep energy for two periods and this power requirement can be met by current electronic technology even in the last few stages. If longer holding time is needed for the last stages such as trapping, a dedicated cooling system may be required.

III. DECELERATION PERFORMANCE

A. Codeceleration and cotrapping of atom-molecular mixture

The codeceleration and cotrapping of a mixture of atomic or/and molecular species provide unique access to sympa-

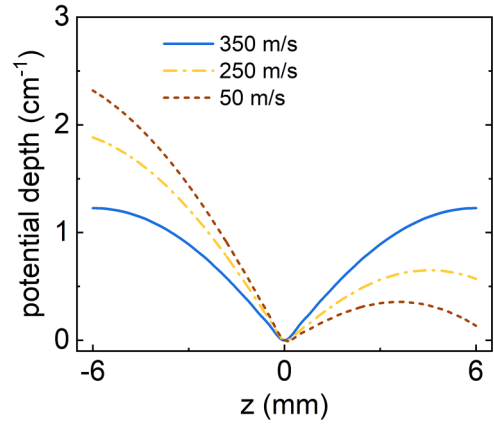


FIG. 3. Deceleration dependence of the pseudo potential well experienced by an O_2 molecule in a 1-meter-long RTWZD. Different final velocities of the moving trap correspond to different accelerations, i.e., 350 m/s (0 km/s^2), 250 m/s (-30.8 km/s^2), 50 m/s (-61.7 km/s^2), respectively.

thetic cooling [59,60] and cold collision studies [55], which have recently been proposed theoretically [61] and demonstrated experimentally [55], where the mixture is decelerated to a very low velocity and is then loaded into a static magnetic trap. Unlike previous works, we directly trap the decelerated mixture of atoms and molecules in the end of the RTWZD without loading processes. Here we quantitatively characterize these dynamic processes with the aid of numerical trajectory calculations.

To achieve this, we use finite-element methods to calculate the contour of several magnetic fields through the cylindrical axis in one period, which allows us to construct the moving potential wells at any time inside the RTWZD by employing interpolation methods. By making certain assumptions in the trajectory calculations, such as ignoring collisions between molecules and removing molecules that exceed the inner diameter of the coil, we use a beam of Li in the $|^2S_{1/2}, J = 1/2, M_S = 1/2\rangle$ state and O_2 in the $|X^3\Sigma_g^-, N = 1, J = 2, M_J = 2\rangle$ state mixture to carry out numerical trajectory simulations. The Zeeman splitting of the two species in applied magnetic fields are shown in Figs. 4(a) and 4(b). The two input beams have the same initial central velocity of 350 m/s and contain the same molecular number of one million. The position and velocity distributions of the incident beam are Gaussian in all directions with the six-dimensional (6D) emittance $[40 \text{ mm} \times 70 \text{ m/s}] \times [4 \text{ mm} \times 30 \text{ m/s}]^2$, where the position and velocity spread are the full width at half maximum (FWHM) of the distributions. These settings in molecular beam are mainly based on recent experimental data [49]. The RTWZD consists of 243 coils and expands to approximately 1.0 m. The time step in the trajectory calculations is $1.0 \times 10^{-7} \text{ s}$.

Figure 4(c) shows the time-of-flight spectrum of the decelerated species, which have a final mean velocity in the range of 350 m/s-10 m/s (the profile of 10 m/s is not shown). Figure 4(d) shows both the transverse and longitudinal phase space distributions of O_2 molecular packets in the end of the decelerator for different final velocities. From Figs. 4(c) and 4(d), it is clear that the longitudinal phase space is fully

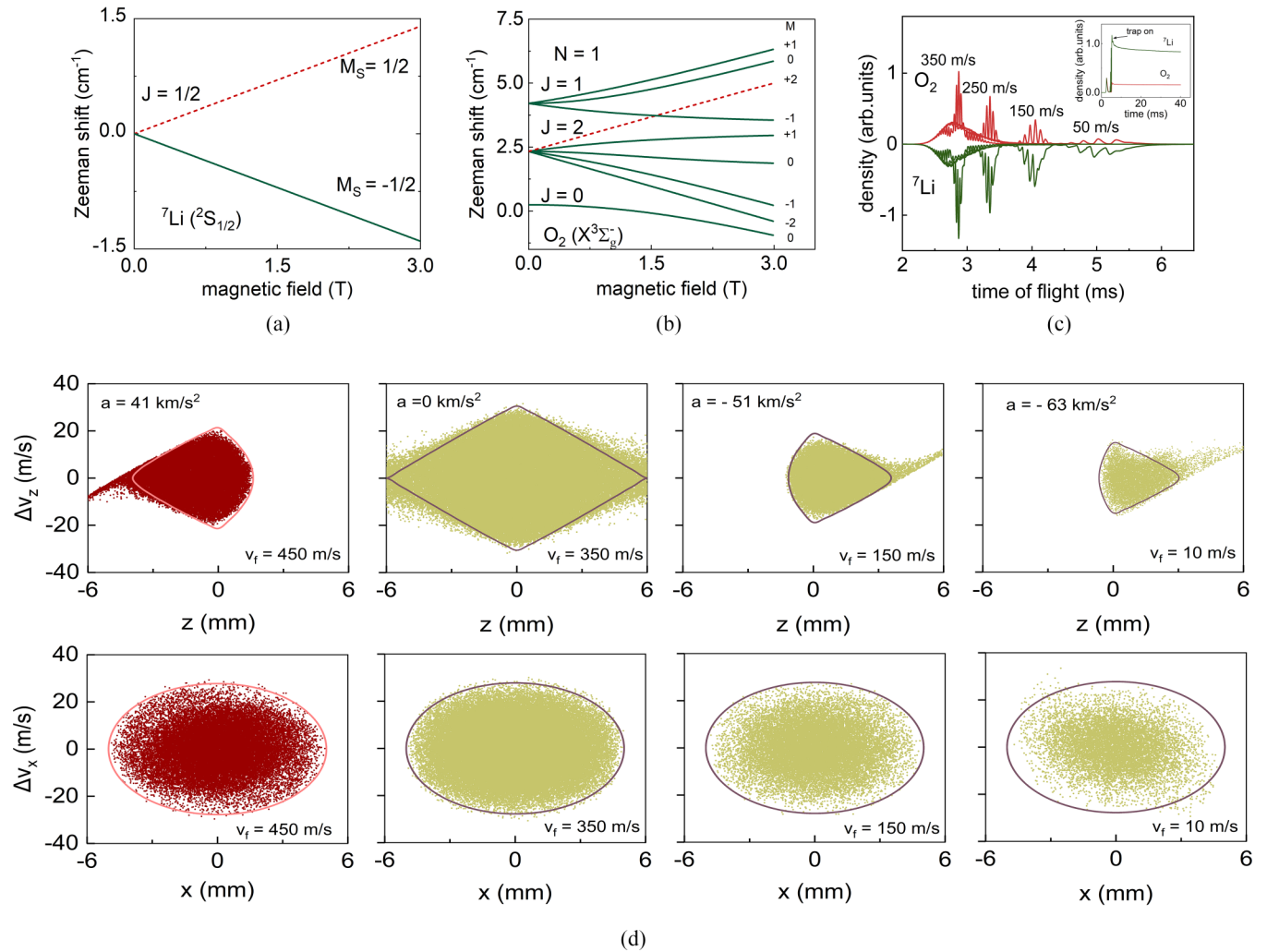


FIG. 4. The Zeeman shift of Li (a) and O_2 (b) in the lowest energy levels as a function of magnetic field strength. (c) The time-of-flight profiles of the mixture of Li and O_2 for different final velocities. Inset shows the time dependence of their number density in the static magnetic trap formed by the last coils. (d) Longitudinal and transverse phase space distributions of O_2 molecules (shown as dots) at the end of the decelerator for various final velocities, together with the separatrices marked by solid circles. These separatrices were calculated using time-averaged potential and force in the decelerator.

occupied at any acceleration, which elucidates the high stability of the RTWZD in the deceleration process. The transverse separatrix, nearly independent of acceleration, is clearly seen at the bottom of Fig. 4(d). Apart from deceleration, the RTWZD performs exceptionally well in accelerating molecules to higher velocities. O_2 molecular packet is accelerated from 350 to 450 m/s, whose phase space distributions are shown in the left segment of Fig. 4(d).

With a slight increase in acceleration to -63.01 km/s^2 , the moving trap and the mixture of Li and O_2 samples can be brought to a standstill at the end of the decelerator. In traditional pulsed Zeeman deceleration [49] and trapping experiments [58], molecular loading processes and associated loading losses are inevitable, even though the traps are situated immediately behind the end of the decelerators. In contrast, once the moving potential of the RTWZD comes to a standstill, it can act as a stationary trap in the laboratory reference frame, avoiding loading loss. The inset of Fig. 4(c)

shows the time dependence of both Li and O_2 intensity in the static trap formed by the last stages of the decelerator, where two samples are simultaneously confined in the same trap for about 35 ms. The velocity spreads (FWHM) of the O_2 and Li samples in the trap are 19.2 and 41.3 m/s, respectively, corresponding to temperatures of 256 and 259 mK, achieved using the theoretical prediction $T = m\Delta v^2 / (8 \ln 2 k_B)$, with m being the molecular mass, Δv the velocity spread, and k_B the Boltzmann constant.

B. Deceleration and trapping of heavy molecules

In order to characterize the performance of the RTWZD for deceleration and trapping of heavy molecules, we test with SrF and YbF since they are heavy, laser-coolable [62,63] molecules of interest to precision measurement and scattering studies [64,65]. A SrF molecular beam was recently decelerated to a standstill from an initial velocity of 190 m/s using a 4.5-m-long TWSD [33], while a YbF beam in the low-

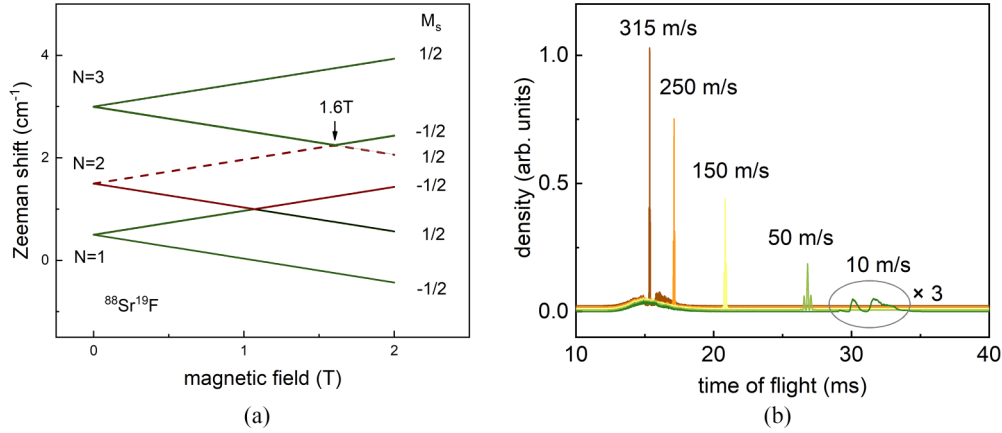


FIG. 5. (a) Zeeman shift of $^{88}\text{Sr}^{19}\text{F}$ of low-lying rotational states. N is the rotational number and M_s is the projection of spin S on the electric field axis. The low-field-seeking state used in the Zeeman deceleration is represented by dashed line. (b) Calculated time-of-flight traces of decelerated $^{88}\text{Sr}^{19}\text{F}$ molecules for different final velocities.

field-seeking state was decelerated from 315 m/s to 280 m/s using the same technique [66]. In this study, we aim to utilize our proposed RTWZD to decelerate and trap $^{88}\text{Sr}^{19}\text{F}$ and $^{174}\text{Yb}^{19}\text{F}$ molecules from supersonic speeds, with the method of trajectory calculation.

For $^{88}\text{Sr}^{19}\text{F}$, the state of $|X^2\Sigma_{1/2}, N=2, M_s=1/2\rangle$ is selected in the following calculations. Figure 5 shows the Zeeman shift of selected $N=1, 2$, and 3 levels of $^{88}\text{Sr}^{19}\text{F}$ in the $|X^2\Sigma_{1/2}, \nu=0\rangle$ state, where the selected level is nearly linear with the increasing applied magnetic field strength until the avoided crossing point (1.6 T). At the maximum magnetic field (1.4 T) on the beam axis, the Zeeman shift is 0.65 cm^{-1} . The incident SrF molecular beam consists of one million molecules with a Gaussian distribution in position and velocity in all directions, and an initial central velocity of 315 m/s. The 6D emittance is $[20\text{ mm} \times 60\text{ m/s}] \times [2\text{ mm} \times 30\text{ m/s}]^2$, where the position and velocity spreads correspond to the FWHM of the distributions, and are based on recent experimental data [67]. The RTWZD contains 1200 coils and expands to 4.8 m. Figure 5 presents the time-of-flight spectrum of SrF beams yielded from the 3D trajectory calculations, where SrF molecules are decelerated to a range of 315 m/s to 10 m/s with different accelerations of the traveling potential wells, namely 0 km/s^2 (315 m/s), -3.8 km/s^2 (250 m/s), -8.0 km/s^2 (150 m/s), -10.0 km/s^2 (50 m/s), and -10.3 km/s^2 (10 m/s).

Once the acceleration increases to -10.33 km/s^2 , the RTWZD can bring SrF to a standstill at the end of the structure. The trap has a size of about $25\pi \times 12\text{ mm}^3$ and a depth of around 0.6 cm^{-1} , capable of confining SrF molecules with velocities below 12 m/s. Figure 6 plots the molecular density in the magnetic trap as a function of the holding time for SrF molecules. The inset in Fig. 6 reveals the phase space distribution of the molecular packet that are confined in the trap for more than 20 ms. The velocity spread (FWHM) of the SrF sample in the trap is 7.7 m/s, corresponding to a temperature of 135 mK. Likewise, the YbF molecular packet has also been stable in confinement by the static magnetic trap formed by the last coils (not shown). The conclusion can be drawn that the RTWZD enables effective deceleration of heavy molecules from supersonic velocities to any desired

velocities and ultimately traps them in the laboratory frame with stability.

IV. DISCUSSION

Since the emerging of the first Zeeman decelerator, many strategies came up to improve phase space acceptance and number of particles that can be decelerated. Limited by the length of this paper, we only give a detailed comparison between our scheme and two other strategies, i.e., the TPZD [45] and the CMZD [68], due to the following reasons. First, they are two of the most representative methods in Zeeman deceleration, where TPZD stands for traditional methods and CMZD stands for true 3D magnetic potential methods. Second, due to their importance and benchmarking in the development of Zeeman deceleration of fast-moving paramagnetic particles, various upgrading methods since then have been compared with them in order to illustrate their improvements [35,40,41,69,70]. For the same reason, we choose to quantitatively compare with them to verify the performance of our scheme.

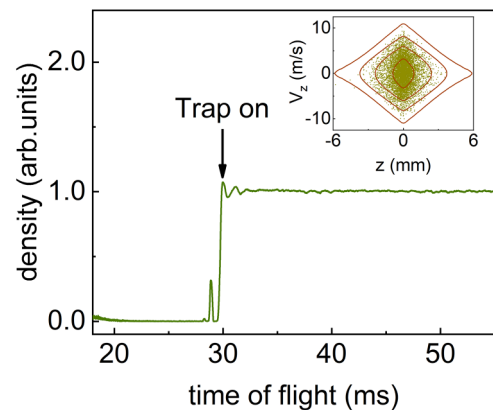


FIG. 6. Density of SrF as a function of the holding time in the static magnetic trap composed by the last coils of the RTWZD. Inset shows the phase space distribution of the SrF molecules in the trap.

TABLE I. List of parameters for the three types of Zeeman decelerators.

Parameters	Symbol	TPZD	CMZD	RTWZD
Stationary magnetic field maximum along symmetry axis	B_{\max}	2.2 T	0.4 T/0.8T	1.4 T
Length of one potential well	$2L/3L$	21.4 mm	10 mm	12 mm
Bore diameter	D	5 mm	10 mm	10 mm
Current	I_0	300 A	600A	750 A
Coil number	N_{stage}	91	200	243
Coil geometry	—	4×16	$2 \times 4/4 \times 4$	5×6
Length of the decelerator	S	1.0 m	1.0 m	1.0 m

In fact, it is challenging to quantitatively compare the performance of different types of Zeeman decelerators due to the numerous factors that influence their efficiency, including coil size, applied currents, selected atom/molecule, and state used. Different experiments also have varying focuses regarding the properties of cold molecular beams. This study concentrates only on phase space acceptance and molecular number produced by the decelerator since they are essential in many experiments involving cold physical and chemical studies.

A. Comparison with the traditional Zeeman decelerator

For the TPZD, we fully adopt the experimental parameters of the Merkt group at ETH Zürich [45]. For the RTWZD, the parameters used are the same as before. The O_2 molecule is selected as an example. Table I lists the parameters utilized in the 1.0 m length decelerators.

Let us first focus on the acceptance of Zeeman decelerators, which indicates the phase space volume occupied by atoms/molecules that can be decelerated to the end. The acceptance of the two kinds of decelerator is shown in Fig. 7(a). The 6D phase space acceptance of both schemes gradually decreases with decreasing final velocities. The acceptance of the TPZD varies between 10^7 ($\text{mm} \times \text{m/s}$)³ and 10^5 ($\text{mm} \times \text{m/s}$)³, whereas the acceptance of the RTWZD is consistently on the order of 10^7 ($\text{mm} \times \text{m/s}$)³. To be precise, the 6D phase space acceptance of the RTWZD is 3 to 50 times higher than that of the TPZD.

We utilize the method of trajectory calculations to obtain a quantitative comparison between the TPZD and the RTWZD. Both decelerators were tested with identical initial

molecular beam parameters and the results are shown in Figs. 7(b) and 7(c). At different final velocities, the RTWZD produced 200 ~ 600 times more cold molecules than the TPZD, and the guiding mode was 40 times more efficient. For a given final velocity of 10 m/s, the RTWZD yields a number of molecules three orders of magnitude higher than the TPZD, as shown in Fig. 7(c).

B. Comparison with 3D potential well Zeeman decelerator

Let us focus on the comparison between the RTWZD and the CMZD. These two types of decelerators have similar size and share the beauty of relative simplicity of the design of the coils. Nevertheless, they are fundamentally distinct in operation and performance. By utilizing the method of trajectory calculation, we compare the performance of the CMZD and the RTWZD, employing O_2 molecule as a tester. Figures 7(b) and 7(c) depict the calculated outcomes, where the parameters of the CMZD have entirely complied with Ref. [36]. As can be seen from these pictures, the CMZD has an excellent performance in slowing down small molecules such as O_2 and yields about two orders of magnitude more molecule than the TPZD. However, the CMZD yields several times fewer molecules than the RTWZD in any case.

Additionally, the $^{174}\text{Yb}^{19}\text{F}$ molecule in the $|X^2\Sigma_{1/2}, N=2, M_s=1/2\rangle$ state is also used to test the RTWZD, which is expanded to 6.4 m (i. e., 1600 coils). The YbF molecular beam comprising one million molecules is brought to 10 m/s from the initial velocity range from 310 m/s to 190 m/s, as depicted in Fig. 8(a). Similar to the case of SrF, the molecular packet of YbF in the moving trap can be stably decelerated to low velocities. Although the survival molecules

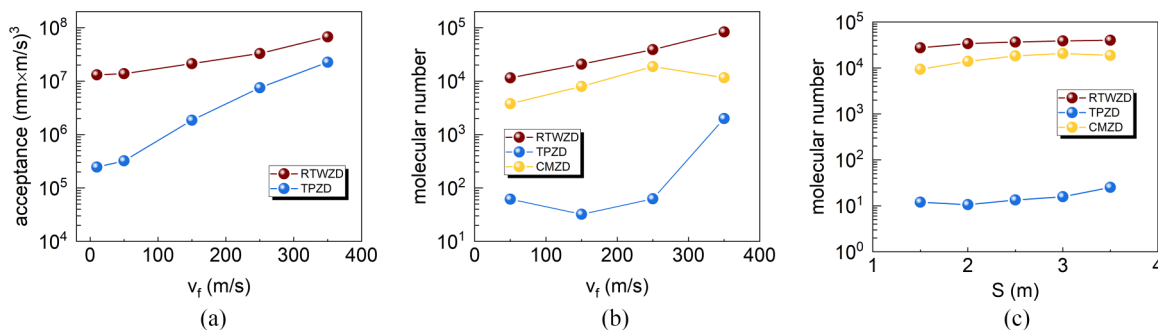


FIG. 7. (a) 6D phase-space acceptance of the RTWZD and TPZD as a function of final velocity. (b) Comparison of the number of molecules yielded from three types of Zeeman decelerator, RTWZD, CMZD, and TPZD, as a function of the final velocity. (c) The relationship between the number of O_2 molecules produced by the RTWZD, CMZD, and TPZD and the decelerator length at a fixed final velocity of 10 m/s.

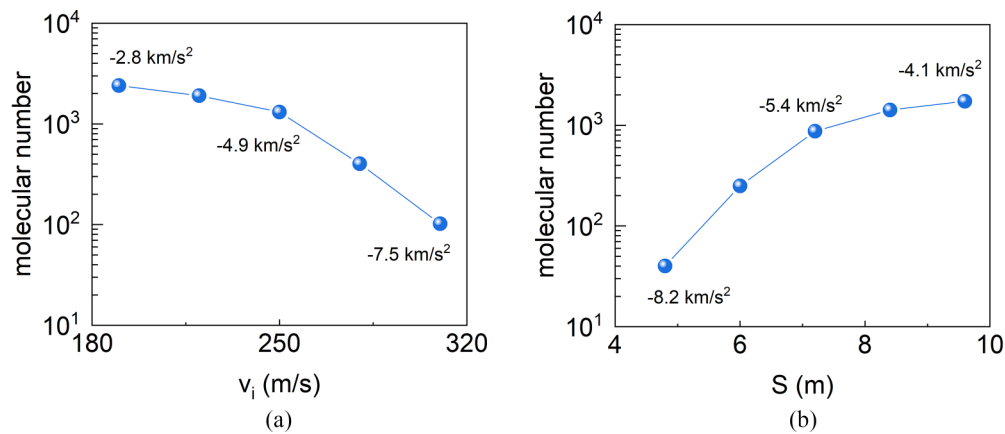


FIG. 8. The number of cold YbF molecules with a mean velocity of 10 m/s obtained by the RTWZD as a function of the initial velocity (a) and the decelerator length (b).

decrease with the increasing accelerations, the stable phase space areas are almost occupied by the YbF molecules in any case. Figure 8(b) shows the deceleration performance of the YbF beam as a function of the decelerator length, with velocity being decelerated from 280 m/s to 10 m/s. When the length of the decelerator expands from 4.8 m to 9.6 m, the number of molecules prepared by the RTWZD increases almost two orders of magnitude. From the above discussions, we conclude that the RTWZD can tame supersonic beams of heavy molecules.

V. CONCLUSIONS

We presented a ring-shaped traveling wave Zeeman decelerator featured with true 3D magnetic potential wells, which enables greatly enhancing the density and quantity of cold atomic/molecular samples. In comparison to the traditional Zeeman decelerator, the phase space acceptance and molecular number can be improved by more than one and two to three orders of magnitude, respectively. The RTWZD is capable of decelerating mixtures of atoms or/and molecules to any desired velocities. It also has a powerful ability to slow down and trap heavy molecules (like SrF and YbF) within the decelerator, which significantly expands the species of atoms

and molecules being decelerated for precision measurement and cold collision.

Incorporating laser cooling techniques [71], with the present Zeeman decelerator can further improve the phase-space density and reduce the temperature of the atomic/molecular samples in the deceleration process. The magnetic trap composed by the last coils of the RTWZD can also provide a platform for a magneto-optical trap or evaporative cooling. Because of the ability to tame a broader range of atomic/molecular species with higher atomic/molecular flux, the present RTWZD offers more possibilities for numerous scenarios such as cold collision, precision measurement, sympathetic cooling [59], laser cooling, and so on.

There are no conflicts of interest to declare.

ACKNOWLEDGMENTS

Project supported by the National Natural Science Foundation of China (Grants No. 91536218, No. 12274140, No. 11834003, and No. 11974434), Shanghai Natural Science Foundation (Grant No. 22ZR1421400), the Program for Professor of Special Appointment (Eastern Scholar) at Shanghai Institutions of Higher Learning, China, and the Young Top-Notch Talent Support Program of Shanghai, China

- [1] M. S. Safronova, D. Budker, D. DeMille, D. F. J. Kimball, A. Derevianko, and C. W. Clark, *Rev. Mod. Phys.* **90**, 025008 (2018).
- [2] C. Cheng, A. P. P. van der Poel, P. Jansen, M. Quintero-Perez, T. E. Wall, W. Ubachs, and H. L. Bethlem, *Phys. Rev. Lett.* **117**, 253201 (2016).
- [3] B. R. Heazlewood and T. P. Softley, *Nat. Rev. Chem.* **5**, 125 (2021).
- [4] V. Andreev *et al.*, *Nature (London)* **562**, 355 (2018).
- [5] Y. V. Stadnik and V. V. Flambaum, *Phys. Rev. Lett.* **115**, 201301 (2015).
- [6] C. Chin, V. V. Flambaum, and M. G. Kozlov, *New J. Phys.* **11**, 055048 (2009).
- [7] D. DeMille, *Phys. Rev. Lett.* **88**, 067901 (2002).
- [8] A. B. Magann, M. D. Grace, H. A. Rabitz, and M. Sarovar, *Phys. Rev. Res.* **3**, 023165 (2021).
- [9] J. D. Weinstein, R. deCarvalho, T. Guillet, B. Friedrich, and J. M. Doyle, *Nature (London)* **395**, 148 (1998).
- [10] D. Egorov, T. Lahaye, W. Schöllkopf, B. Friedrich, and J. M. Doyle, *Phys. Rev. A* **66**, 043401 (2002).
- [11] N. R. Hutzler, H. I. Lu, and J. M. Doyle, *Chem. Rev.* **112**, 4803 (2012).
- [12] T. Junglen, T. Rieger, S. A. Rangwala, P. W. H. Pinkse, and G. Rempe, *Phys. Rev. Lett.* **92**, 223001 (2004).
- [13] T. Rieger, T. Junglen, S. A. Rangwala, G. Rempe, P. W. H. Pinkse, and J. Bulthuis, *Phys. Rev. A* **73**, 061402(R) (2006).
- [14] J. Toscano, M. Hejduk, H. G. McGhee, and B. R. Heazlewood, *Rev. Sci. Instrum.* **90**, 033201 (2019).

- [15] M. Gupta and D. Herschbach, *J. Phys. Chem. A* **103**, 10670 (1999).
- [16] S. Chervenkov, X. Wu, J. Bayerl, A. Rohlfes, T. Gantner, M. Zeppenfeld, and G. Rempe, *Phys. Rev. Lett.* **112**, 013001 (2014).
- [17] H. L. Bethlem, G. Berden, and G. Meijer, *Phys. Rev. Lett.* **83**, 1558 (1999).
- [18] E. Narevicius, C. G. Parthey, A. Libson, M. F. Riedel, U. Even, and M. G. Raizen, *New J. Phys.* **9**, 96 (2007).
- [19] E. Vliegen, H. J. Wörner, T. P. Softley, and F. Merkt, *Phys. Rev. Lett.* **92**, 033005 (2004).
- [20] R. Fulton, A. I. Bishop, and P. F. Barker, *Phys. Rev. Lett.* **93**, 243004 (2004).
- [21] D. McCarron, *J. Phys. B* **51**, 212001 (2018).
- [22] J.-R. Li *et al.*, *Nat. Phys.* **17**, 1144 (2021).
- [23] P. D. Lett, K. Helmerson, W. D. Phillips, L. P. Ratliff, S. L. Rolston, and M. E. Wagshul, *Phys. Rev. Lett.* **71**, 2200 (1993).
- [24] J. D. Miller, R. A. Cline, and D. J. Heinzen, *Phys. Rev. Lett.* **71**, 2204 (1993).
- [25] D. Mitra, K. H. Leung, and T. Zelevinsky, *Phys. Rev. A* **105**, 040101 (2022).
- [26] P. Aggarwal *et al.*, *Rev. Sci. Instrum.* **92**, 033202 (2021).
- [27] S. Y. T. van de Meerakker, N. Vanhaecke, H. L. Bethlem, and G. Meijer, *Phys. Rev. A* **73**, 023401 (2006).
- [28] B. C. Sawyer, B. K. Stuhl, B. L. Lev, J. Ye, and E. R. Hudson, *Eur. Phys. J. D* **48**, 197 (2008).
- [29] S. Y. T. van de Meerakker, N. Vanhaecke, H. L. Bethlem, and G. Meijer, *Phys. Rev. A* **71**, 053409 (2005).
- [30] S. A. Meek, H. Conrad, and G. Meijer, *Science* **324**, 1699 (2009).
- [31] S. A. Meek, M. F. Parsons, G. Heyne, V. Platschkowski, H. Haak, G. Meijer, and A. Osterwalder, *Rev. Sci. Instrum.* **82**, 093108 (2011).
- [32] M. Quintero-Perez, P. Jansen, T. E. Wall, J. E. van den Berg, S. Hoekstra, and H. L. Bethlem, *Phys. Rev. Lett.* **110**, 133003 (2013).
- [33] P. Aggarwal *et al.*, *Phys. Rev. Lett.* **127**, 173201 (2021).
- [34] T. Cremers, S. Chefdeville, N. Janssen, E. Sweers, S. Koot, P. Claus, and S. Y. T. van de Meerakker, *Phys. Rev. A* **95**, 043415 (2017).
- [35] J. Toscano, L. Y. Wu, M. Hejduk, and B. R. Heazlewood, *J. Phys. Chem. A* **123**, 5388 (2019).
- [36] E. Lavert-Ofir, L. David, A. B. Henson, S. Gersten, J. Narevicius, and E. Narevicius, *Phys. Chem. Chem. Phys.* **13**, 18948 (2011).
- [37] N. Akerman, M. Karpov, L. David, E. Lavert-Ofir, J. Narevicius, and E. Narevicius, *New J. Phys.* **17**, 065015 (2015).
- [38] A. Trimeche, M. N. Bera, J. P. Cromieres, J. Robert, and N. Vanhaecke, *Eur. Phys. J. D* **65**, 263 (2011).
- [39] L. A. Mcard, A travelling wave Zeeman decelerator for atoms and molecules, Ph.D. thesis, Durham University (2018).
- [40] T. Damjanović, S. Willitsch, N. Vanhaecke, H. Haak, G. Meijer, J.-P. Cromières, and D. Zhang, *New J. Phys.* **23**, 105006 (2021).
- [41] T. Damjanović, S. Willitsch, N. Vanhaecke, H. Haak, G. Meijer, J. Cromières, and D. Zhang, *New J. Phys.* **23**, 105007 (2021).
- [42] S. D. Hogan, D. Sprecher, M. Andrist, N. Vanhaecke, and F. Merkt, *Phys. Rev. A* **76**, 023412 (2007).
- [43] K. Dulitz, A. Tauschinsky, and T. P. Softley, *New J. Phys.* **17**, 035005 (2015).
- [44] L. Semeria, P. Jansen, G. Clausen, J. A. Agner, H. Schmutz, and F. Merkt, *Phys. Rev. A* **98**, 062518 (2018).
- [45] A. W. Wiederkehr, M. Motsch, S. D. Hogan, M. Andrist, H. Schmutz, B. Lambillotte, J. A. Agner, and F. Merkt, *J. Chem. Phys.* **135**, 214202 (2011).
- [46] K. Dulitz, J. Toscano, A. Tauschinsky, and T. P. Softley, *J. Phys. B* **49**, 075203 (2016).
- [47] V. Plomp, X.-D. Wang, F. Lique, J. Klos, J. Onvlee, and S. Y. T. van de Meerakker, *J. Phys. Chem. Lett.* **12**, 12210 (2021).
- [48] A. W. Wiederkehr, H. Schmutz, M. Motsch, and F. Merkt, *Mol. Phys.* **110**, 1807 (2012).
- [49] Y. Liu, S. Zhou, W. Zhong, P. Djuricanin, and T. Momose, *Phys. Rev. A* **91**, 021403(R) (2015).
- [50] T. Cremers, S. Chefdeville, V. Plomp, N. Janssen, E. Sweers, and S. Y. T. van De Meerakker, *Phys. Rev. A* **98**, 033406 (2018).
- [51] V. Plomp, Z. Gao, T. Cremers, and S. Y. T. van de Meerakker, *Phys. Rev. A* **99**, 033417 (2019).
- [52] V. Plomp, Z. Gao, T. Cremers, M. Besemer, and S. Y. T. van de Meerakker, *J. Chem. Phys.* **152**, 091103 (2020).
- [53] T. Momose, Y. Liu, S. Zhou, P. Djuricanin, and D. Carty, *Phys. Chem. Chem. Phys.* **15**, 1772 (2013).
- [54] Y. Liu, M. Vashishta, P. Djuricanin, S. Zhou, W. Zhong, T. Mittertreiner, D. Carty, and T. Momose, *Phys. Rev. Lett.* **118**, 093201 (2017).
- [55] Y. Segev, M. Pitzer, M. Karpov, N. Akerman, J. Narevicius, and E. Narevicius, *Nature (London)* **572**, 189 (2019).
- [56] Y. Liu and L. Luo, *Front. Phys.* **16**, 42300 (2021).
- [57] M. R. Tarbutt, J. J. Hudson, B. E. Sauer, and E. A. Hinds, *Farad. Discuss.* **142**, 37 (2009).
- [58] E. Narevicius, A. Libson, C. G. Parthey, I. Chavez, J. Narevicius, U. Even, and M. G. Raizen, *Phys. Rev. A* **77**, 051401(R) (2008).
- [59] M. Morita, M. B. Kosicki, P. S. Żuchowski, and T. V. Tscherebul, *Phys. Rev. A* **98**, 042702 (2018).
- [60] A. O. G. Wallis and J. M. Hutson, *Phys. Rev. Lett.* **103**, 183201 (2009).
- [61] Y. Liu and L. Luo, *Front. Phys.* **16**, 12504 (2021).
- [62] E. S. Shuman, J. F. Barry, and D. Demille, *Nature (London)* **467**, 820 (2010).
- [63] J. Lim, J. R. Almond, M. A. Trigatzis, J. A. Devlin, N. J. Fitch, B. E. Sauer, M. R. Tarbutt, and E. A. Hinds, *Phys. Rev. Lett.* **120**, 123201 (2018).
- [64] J. J. Hudson, B. E. Sauer, M. R. Tarbutt, and E. A. Hinds, *Phys. Rev. Lett.* **89**, 023003 (2002).
- [65] L. D. Carr, D. DeMille, R. V. Krems, and J. Ye, *New J. Phys.* **11**, 055049 (2009).
- [66] N. E. Bulleid, R. J. Hendricks, E. A. Hinds, S. A. Meek, G. Meijer, A. Osterwalder, and M. R. Tarbutt, *Phys. Rev. A* **86**, 021404(R) (2012).
- [67] S. C. Mathavan, A. Zapara, Q. Esajas, and S. Hoekstra, *ChemPhysChem* **17**, 3709 (2016).
- [68] N. Akerman, M. Karpov, Y. Segev, N. Bibelnik, J. Narevicius, and E. Narevicius, *Phys. Rev. Lett.* **119**, 073204 (2017).
- [69] J. Toscano, A. Tauschinsky, K. Dulitz, C. J. Rennick, B. R. Heazlewood, and T. P. Softley, *New J. Phys.* **19**, 083016 (2017).
- [70] A. W. Wiederkehr, S. D. Hogan, and F. Merkt, *Phys. Rev. A* **82**, 043428 (2010).
- [71] T. E. Wall, J. F. Kanem, J. M. Dyne, J. J. Hudson, B. E. Sauer, E. A. Hinds, and M. R. Tarbutt, *Phys. Chem. Chem. Phys.* **13**, 18991 (2011).